Spectrochimica Acta Part A: Molecular and Biomolecular Spectroscopy 192 (2018) 128–139

Contents lists available at ScienceDirect

Spectrochimica Acta Part A: Molecular and Biomolecular Spectroscopy

journal homepage: www.elsevier.com/locate/saa

# Human serum albumin binding of certain antimalarials

Olivera S. Marković [a], Ilija N. Cvijetić [b], Mario V. Zlatović [c], Igor M. Opsenica [c], Jelena M. Konstantinović [c], Nataša V. Terzić Jovanović [a], Bogdan A. Šolaja [c,d], Tatjana Ž. Verbić [c,*]

[a] Department of Chemistry-IChTM, University of Belgrade, Njegoševa 12, 11000 Belgrade, Serbia
[b] Innovation Center of the Faculty of Chemistry, University of Belgrade, Studentski trg 12-16, 11000 Belgrade, Serbia
[c] Faculty of Chemistry, University of Belgrade, Studentski trg 12-16, 11000 Belgrade, Serbia
[d] Serbian Academy of Sciences and Arts, Knez Mihailova 35, 11000 Belgrade, Serbia

ARTICLE INFO

*Article history:*
Received 8 May 2017
Received in revised form 9 October 2017
Accepted 23 October 2017
Available online xxxx

*Keywords:*
Aminoquinolines
Human serum albumin
Fluorescence spectroscopy
Binding affinity
Molecular docking
Stern-Volmer plot

ABSTRACT

Interactions between eight in-house synthesized aminoquinolines, along with well-known chloroquine, and human serum albumin (HSA) have been studied by fluorescence spectroscopy. The synthesized aminoquinolines, despite being structurally diverse, were found to be very potent antimalarials. Fluorescence measurements indicate that three compounds having additional thiophene or benzothiophene substructure bind more strongly to HSA than other studied compounds. Competitive binding experiments indicate that these three compounds bind significantly stronger to warfarin compared to diazepam binding site. Fluorescence quenching at three temperatures (20, 25, and 37 °C) was analyzed using classical Stern-Volmer equation, and a static quenching mechanism was proposed. The enthalpy and entropy changes upon sulphur-containing compound–HSA interactions were calculated using Van't Hoff equation. Positive values of enthalpy and entropy changes indicate that non-specific, hydrophobic interactions are the main contributors to HSA–compound interaction. Molecular docking and calculated lipophilicity descriptors indicate the same, pointing out that the increased lipophilicity of sulphur-containing compounds might be a reason for their better binding to HSA. Obtained results might contribute to design of novel derivatives with improved pharmacokinetic properties and drug efficacy.
© 2017 Elsevier B.V. All rights reserved.

## 1. Introduction

Human serum albumin (HSA) is single-chain, non-glycosylated polypeptide that contains 585 amino acids with molecular weight of 66,500 Da [1] (Fig. 1). The polypeptide chain forms a heart-shaped structure that is composed of three structurally similar α-helical domains (I, II and III) and each of them consists of two subdomains (A and B). HSA has a role in osmotic pressure and pH regulation, sequestering oxygen free radicals, inactivating various toxic lipophilic metabolites and transport of endogenous (fatty acids, hormones, bile acids, amino acids) and exogenous compounds (drug molecules and nutrients). It is shown that HSA (concentration in serum approximately 0.6 mM [1]) is a major binder of acidic drug molecules in plasma, unlike alpha-1-acid glycoprotein (AGP, concentration in serum approximately 20 μM [2]) which binds mainly basic drug molecules. Also, negatively charged compounds bind more strongly to HSA than positively charged ones [3].

Most drugs bind primarily to two specific binding sites on HSA. The site I (warfarin binding site) and site II (also called the indole-benzodiazepine site) are located in domains IIA and IIIA (Fig. 1), respectively [5]. Ligands that strongly bind to site I are dicarboxylic acids and/or bulky heterocyclic molecules with a negative charge localized in the middle of the molecule. Such ligands are warfarin, azapropazone, phenylbutazone, *etc.* Low stereoselectivity of this site toward small organic molecules might be ascribed to its flexibility. Ligands that bind to site II are generally aromatic carboxylic acids, with a negative charge located distant from the hydrophobic region of the molecule, like diazepam, diflunisal, and ibuprofen. Sudlow site II is smaller, but topologically similar to site I. Site II appears to be less flexible, since ligand binding often shows stereoselectivity, and is strongly affected by small structural modifications of the ligand. However, these structural features are not strict prerequisites for the site I and site II binding, since numerous ligands are known to bind to both drug binding sites, though with different affinities [6].

The nature and magnitude of HSA–drug interactions affect the pharmacological behavior and side effects of a drug. Strong binding between HSA and drug decreases the concentration of free drug in the blood, and thus decreases the pharmacological effect of a drug (only free drug in the tissues is able to bind to the target receptor). Weak binding leads to a short drug lifetime and its' poor tissue distribution. Connection

* Corresponding author.
*E-mail addresses:* olivera.markovic@ihtm.bg.ac.rs (O.S. Marković), ilija@chem.bg.ac.rs (I.N. Cvijetić), mario@chem.bg.ac.rs (M.V. Zlatović), igorop@chem.bg.ac.rs (I.M. Opsenica), jelena_konstantinovic@chem.bg.ac.rs (J.M. Konstantinović), nterzic@chem.bg.ac.rs (N.V. Terzić Jovanović), bsolaja@chem.bg.ac.rs (B.A. Šolaja), tatjanad@chem.bg.ac.rs (T.Ž. Verbić).

https://doi.org/10.1016/j.saa.2017.10.061
1386-1425/© 2017 Elsevier B.V. All rights reserved.

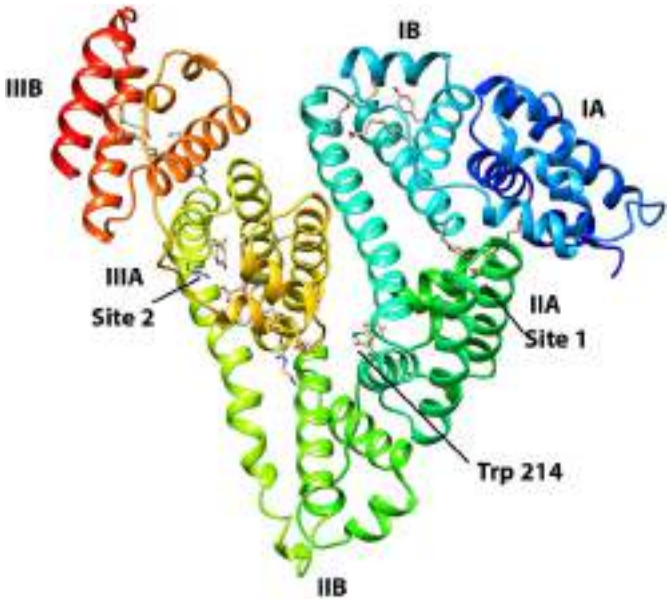


**Fig. 1.** Crystal structure of HSA (PDB ID 1BJ5) and the location of major binding sites. The image is made in Chimera [4].

between free drug concentration in plasma and free drug concentration in tissues can be used in designing the administration regimen dose and establishing the safety margins [7]. As drug binding to HSA and plasma proteins (PP) can be affected by some diseases, information about drug–PP binding might be useful in therapy [5]. Hence, HSA–drug interactions studies provide important information which can be used in pharmaceutical industry in pharmacokinetic (PK) and pharmacodynamic drug profiling.

Interaction between drugs and HSA can be studied by different instrumental techniques: Fourier transform infrared spectroscopy (FTIR), nuclear magnetic resonance spectroscopy (NMR), isothermal titration calorimetry (ITC), UV–Vis and fluorescence spectroscopy, circular dichroism spectroscopy (CD), high-performance liquid chromatography (HPLC), equilibrium dialysis *etc.* [3,8–21].

Fluorescence measurements are often used to study drug to protein binding because the variety of information on the binding mechanism, mode, constants, binding sites, intermolecular distances, *etc.*, can be easily obtained. HSA, as the majority of other proteins, has three fluorophores: tryptophan, tyrosine, and phenylalanine, but its' fluorescence almost exclusively originates from tryptophan 214 alone (Trp214, Fig. 1). Phenylalanine has a very low quantum yield and the fluorescence of tyrosine is almost entirely quenched if it is near to an amino group, a carboxyl group, or a tryptophan. As binding of a drug to HSA occurs, the microenvironment of Trp214 is changed, and the changes of HSA intrinsic fluorescence intensity are induced [22].

Although X-ray diffraction is used as the golden standard for determining protein and protein-ligand complexes structures, computational methods, like molecular docking, are nowadays often used for studying the protein-ligand interactions as well. In cases where structure of the protein is well known, like the structure of HSA is, the binding of various small molecules to the protein binding site can be successfully investigated using molecular modeling.

Chloroquine (CQ) is drug commonly used in the prevention and treatment of malaria and in the treatment of rheumatoid arthritis and influenza. CQ is one of the oldest, cheapest, and easily available synthetic agents used to cure malaria. No drugs have been found possessing the same pharmacological profiles as CQ. Thus, although CQ-resistance against different strains of malarial parasite strains worldwide was reported, many research groups are continuously working on the CQ core structure modification to get new efficient drug [23].

In the search for novel antimalarials with improved PK profile, we explored interactions of CQ and our eight derivatives of CQ (Fig. 2) with HSA using spectroscopic and molecular modeling techniques. The synthesized compounds, despite being structurally diverse, possess aminoquinoline moiety as pharmacophore and they have been found to be very potent nontoxic antimalarials *in vitro* and *in vivo* [24–27]. It is expected that obtained results will be valuable for the design of novel derivatives with improved PK properties and drug efficacy.

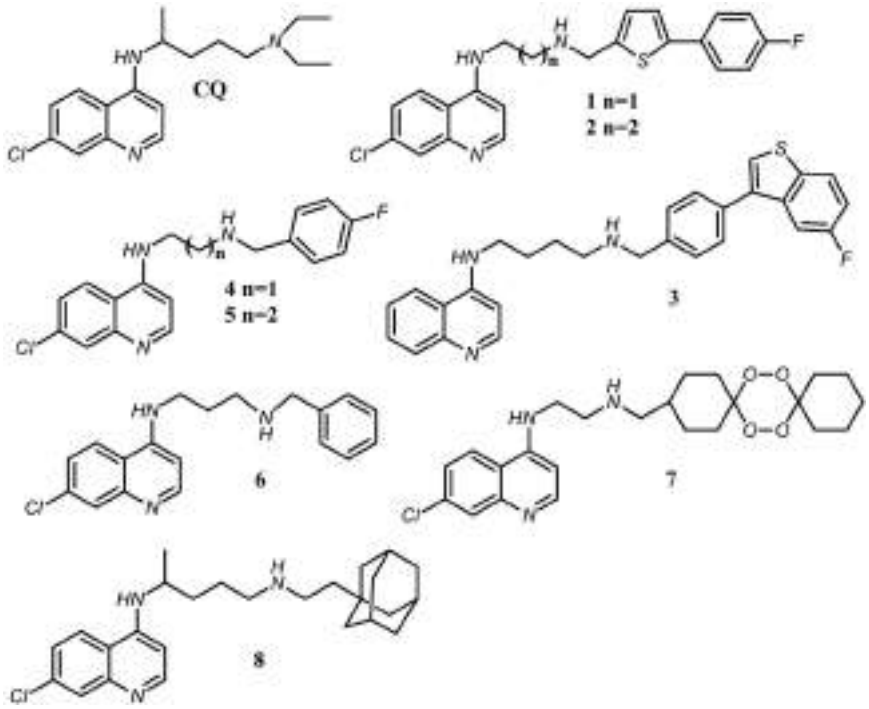


**Fig. 2.** Structures of chloroquine (CQ) and compounds **1–8**.

## 2. Experimental

### 2.1. Material and Methods

HSA was purchased from Sigma-Aldrich. Phosphate buffered saline (pH 7.40; 30 mM; PBS) was used to maintain the physiological pH value (pH 7.40). Potassium dihydrogen phosphate, disodium hydrogen phosphate, sodium chloride, potassium chloride used for PBS preparation, as well as chloroquine diphosphate, were purchased from Sigma-Aldrich. All solutions were prepared with Millipore water.

Fluorescence spectra were recorded on Horiba Jobin Yvon Fluoromax-4 spectrometer, equipped with Peltier element and magnetic stirrer for cuvette, using quartz cell with 1 cm path length and 4 mL volume. An excitation wavelength was 280 nm, with 5 nm slits; emission spectra were recorded in 300–450 nm wavelength range, with 5 nm slits, and 0.1 s integration time. Background PBS signal was subtracted from each spectrum.

UV–Vis spectra were recorded on Thermo scientific spectrophotometer evolution 60s using quartz cell with 1 cm path length and 4 mL volume. All spectra were recorded against the corresponding blank (PBS) in the 300–450 nm wavelength range, with 500 nm/min scan speed.

pH Values were potentiometrically measured using Crison pH-Burette 24 2S equipped with a micro-combined pH electrode (Crison pH electrode 50 29). The pH electrode was calibrated by standard Crison buffer solutions (pH 4.01, 7.00, and 9.21).

### 2.2. Fluorescence and UV–vis Spectra

Stock solutions of HSA ($c = (1.03–1.80) \times 10^{-4}$ M) and CQ·$2H_3PO_4$ ($c = 5.82 \times 10^{-4}$ M) were prepared in 30 mM PBS, pH 7.40, and kept in the refrigerator. Stock solutions of **1** ($c = 2.67 \times 10^{-3}$ M), **2** ($c = 2.19 \times 10^{-3}$ M), **3** ($c = 1.90 \times 10^{-3}$ M), **4** ($c = 1.37 \times 10^{-3}$ M), **5** ($c = 1.26 \times 10^{-3}$ M), **6** ($c = 9.46 \times 10^{-4}$ M), **7** ($c = 8.12 \times 10^{-4}$ M), **8** ($c = 7.82 \times 10^{-4}$ M), warfarin ($c = 1.84 \times 10^{-3}$ M) and diazepam ($c = 2.69 \times 10^{-3}$ M) were prepared in DMSO.

For HSA–compound interaction studies, HSA solution was freshly prepared from the stock, by dilution with a buffer (HSA concentration was kept constant, $c = 5 \times 10^{-7}$ M). Then the HSA solution was titrated with 0.56–2.58 μL increments of compounds' stock solution going from 1 to 15–16 compound/HSA molar ratio. During the titration, the solution was stirred and kept at constant temperature ($t_1 = 20.0 \pm 0.1$ °C (293 K), $t_2 = 25.0 \pm 0.1$ °C (298 K), and $t_3 = 37.0 \pm 0.1$ °C (310 K), regulated by Peltier element). The equilibration time between increment additions was 15 min.

For displacement experiments, HSA and site specific probes (warfarin–Wf and diazepam–Dz) were freshly prepared from the stock, by dilution with a buffer (HSA and site probe concentrations were kept constant ($c = 5 \times 10^{-7}$ M), the equilibration time was 60 min). Then the HSA–Wf/Dz solution was titrated with 0.56–0.79 μL increments of compounds' stock solution going from 1 to 15 compound/complex (HSA–Wf/Dz) molar ratio. During the titration, the solution was stirred and thermostated ($t = 25.0 \pm 0.1$ °C (298 K)), regulated by Peltier element). The equilibration time between increment additions was 15 min.

### 2.3. Synthesis and Characterization

The syntheses and characterization of **1**, **2**, and **4–8** have been previously reported [24–27].

#### 2.3.1. N-[4-(5-Fluoro-1-Benzothien-3-Yl)Benzyl]-N′-Quinolin-4-Ylbutane-1,4-Diamine (3)

*2.3.1.1. General Information.* IR spectrum was recorded on a Thermo-Scientific Nicolet 6700 FT-IR diamond crystal spectrophotometer. $^1$H and $^{13}$C NMR spectra (SM, Fig. S1) were recorded on a Bruker Ultrashield Advance III spectrometer (at 500 and 125 MHz, respectively) in $CDCl_3$ as solvent, using TMS as the internal standard. Chemical shifts are expressed in ppm ($\delta$) values and coupling constants ($J$) in Hz. ESI-MS (HRMS) spectrum of the synthesized compound was acquired on a Agilent Technologies 1200 Series instrument equipped with Zorbax Eclipse Plus C18 (100 × 2.1 mm i.d. 1.8 μm) column and DAD detector (190–450 nm) in combination with a 6210 Time-of-Flight LC/MS instrument in positive ion mode. The sample was dissolved in MeOH (HPLC grade). The selected values were as follows: capillary voltage 4 kV; gas temperature 350 °C; drying gas 12 L/min; nebulizer pressure 45 psig; fragmentator voltage: 70 V. Compound was analyzed for purity (HPLC) using an Agilent 1200 HPLC system equipped with Quat Pump (G1311B), Injector (G1329B) 1260 ALS, TCC 1260 (G1316A) and Detector 1260 DAD VL+ (G1315C). HPLC analysis was performed in two diverse systems (SM, Fig. S2): **Method A:** Zorbax Eclipse Plus C18 4.6 × 150 mm, 1.8 μm, S.N. USWKY01594 was used as the stationary phase. Eluent was made from the following solvents: 0.2% formic acid in water (A) and methanol (B). The analysis was performed at the UV max of the compound (250 nm) to maximize selectivity. Compound was dissolved in methanol, final concentration was ~1 mg/mL. Flow rate was 0.5 mL/min. Compound **3** was eluted using gradient protocol: 0–1 min 95%A, 1–6 min 95%A → 5%A, 6–11 min 5%A, 11–14 min 5%A → 95%A, 14–17 min 95%A. **Method B:** Zorbax Eclipse Plus C18 4.6 × 150 mm, 1.8 μm, S.N. USWKY01594 was used as the stationary phase. Eluent was made from the following solvents: 0.2% formic acid in water (A) and acetonitrile (B)·The analysis was performed at the UV max of the compound (330 nm) to maximize selectivity. Compound was dissolved in methanol, final concentration was ~1 mg/mL. Flow rate was 0.5 mL/min. Compound **3** was eluted using gradient protocol: 0–1.5 min 95%A, 1–5 min 95%A → 5%A, 5–16 min 5%A, 16–18 min 5%A → 95%A, 18–20 min 95%A.

Reaction scheme:

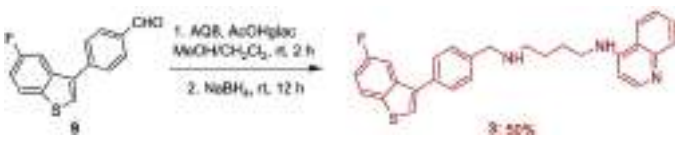


*2.3.1.2. Synthesis.* Aldehyde **9** [28] (158 mg, 0.615 mmol) and amine **AQ8** [27] (199 mg, 0.923 mmol) were dissolved in MeOH/$CH_2Cl_2$ mixture ($v$:$v$; 2:1, 24 mL), glac. AcOH (53 μL, 0.92 mmol) was added, and the mixture was stirred at r.t. After 2 h, $NaBH_4$ (139.6 mg, 3.690 mmol) was added, and stirring was continued for another 12 h. Solvent was removed under reduced pressure, and the residue dissolved in $CH_2Cl_2$. The organic layer was washed with 2 M $NH_4OH$ and then extracted with $CH_2Cl_2$. The combined organic layers were washed with brine and dried over anh. $Na_2SO_4$. Finally, the solvent was evaporated under reduced pressure. The product was purified using column chromatography (dry-flash, $SiO_2$, eluent hexane/EtOAc gradient 1/1 → EtOAc, EtOAc/MeOH gradient 95/5 → 4/6 and flash, Biotage SP1, NH column, eluent DCM/hexane gradient 8/2 → DCM, DCM/MeOH gradient 95/5 → MeOH). Final product (**3**) was obtained as a pale yellow oil (140 mg, 50%). IR (ATR): 3241 w, 3067 w, 2929 w, 2855 w, 1579s, 1538 m, 1494 w, 1437 m, 1398 w, 1373 w, 1339 w, 1251 w, 1194 w, 1126 w, 763 w, 650 w, 542w cm$^{-1}$. $^1$H NMR (500 MHz, $CDCl_3$, $\delta$): 8.55 (d, $J$ = 5.2, H-C(2′)), 7.99–7.95 (m, H-C(8′)), 7.83 (dd, $J_1$ = 4.8, $J_2$ = 8.7, H-C(7)), 7.75–7.72 (m, H-C(5′)), 7.62–7.57 (m, H-C(7′)), 7.57–7.54 (m, H-C(4)), 7.54–7.50 (m, 2H-Ar), 7.47–7.43 (m, 3H, 2H-Ar and H-C(2)), 7.35–7.31 (m, H-C(6′)), 7.17–7.12 (m, H-C(6)), 6.41 (d, $J$ = 5.5, H-C(3′)), 5.69 (bs, H-N exchangeable with $D_2O$), 3.90 (s, 2H,

ArC$H_2$-), 3.38–3.32 (m, 2H, ArNHC$H_2$-), 2.80 (t, 2H, $J$ = 6.8, ArCH$_2$NHC$H_2$-), 1.94–1.87 (m, 2H, ArNHCH$_2$C$H_2$-), 1.78–1.63 (m, 3H, ArCH$_2$NHCH$_2$C$H_2$- and H-N exchangeable with $D_2O$)·$^{13}$C NMR (125 MHz, $CDCl_3$, $\delta$): 161.10 (d, $J$ = 240.1), 151.02, 149.84, 148.38, 139.80, 139.09 (d, $J$ = 9.5), 137.59 (d, $J$ = 4.5), 135.98, 134.30, 129.87, 128.92, 128.58, 128.56, 125.62, 124.41, 123.99 (d, $J$ = 9.5), 119.51, 118.80, 113.33 (d, $J$ = 25.3), 108.51 (d, $J$ = 23.5), 98.64, 53.72, 48.76, 43.20, 27.79, 26.47. HRMS: $m/z$ 456.19032 corresponds to molecular formula $C_{28}H_{26}N_3SFH^+$ (error in ppm −0.22). HPLC purity: method A (λ = 250 nm): RT 12.236, area 95.18%; method B (λ = 330 nm): RT 7.869, area 98.42%.

### 2.4. Computational Details

As a protein model, we used crystal structure of HSA with R-warfarin (PDB code 1H9Z [29]). For protein preparation, Protein Preparation Wizard from Schrödinger Suite 2014-1 was used. All structures and their images were prepared, visualized and hard copied using Maestro, version 9.7, Schrödinger, LLC, New York, NY, 2014. For ligand preparation and *in silico* p$K_a$ prediction we used Epik, version 2.7, Schrödinger, LLC, New York, NY, 2014. All ligands were docked as protonated, since p$K_a$ values predictions from Epik suggested that on physiological pH, both secondary aliphatic nitrogen and chloroquine/quinoline nitrogen are protonated. In our docking simulations we used the binding site of warfarin as a binding site center. Flexible ligand docking was performed in Glide from Schrodinger Suite using QM-Polarized Ligand Docking protocol. Ligands were docked in binding site using *ab initio* calculated charges in water as a solvent and final pose selection was done by glide docking score function. [Schrodinger Suite 2014-1; Glide version 5.9, Jaguar version 8.0, QSite version 5.9, Schrödinger, LLC, New York, NY, 2014.]

Binding energies were calculated using Prime MM-GBSA [30] from Schrodinger Suite, using variable-dielectric generalized Born model of solvation and OPLS-2005 force field, with flexible residues on 6 Å from ligand.

After preparation of protein model, molecules **1–3** and **8** were submitted to QM-polarized ligand docking.

Initial conformations of CQ and compounds **1–8** used for lipophilicity calculations were lowest energy ones obtained in OMEGA 2.5.1.4 program [31]. Those geometries are further refined through geometry optimizations in MOPAC2016 [32], using a semiempirical PM6 method [33]. The values of lipophilicity descriptors are calculated using built-in tools in VegaZZ software [34].

**Table 1**
*In vitro* antiplasmoidal activity of compound **3** against *P. falciparum* strains.

| Compound | *In vitro* antimalarial activity (*P. falciparum*, $IC_{50}$, nM)[a,b] | | | HepG2[f] $IC_{50}$ (nM) | SI[g] HepG2/D6 |
|---|---|---|---|---|---|
| | D6[c] | W2[d] | TM91C235[e] | | |
| 3 | 11 | 125 | 147 | 2360 | 214 |
| CQ[h] | 15 (6) | 595 (5) | 206 (5) | | |
| MFQ[h] | 23 (6) | 7 (5) | 55 (5) | | |

[a] Antiplasmodial $IC_{50}$ values (nM) (Malaria SYBR Green Fluorescence Assay) for isolates and clones of *P. falciparum*.
[b] In vitro experiments for compound **3** were done as technical quadruplicates, mean values are given.
[c] CQ susceptible *P. falciparum* African D6 clone.
[d] CQ resistant *P. falciparum* Indochina W2 clone.
[e] *P. falciparum* multidrug resistant C235 strain (Thailand).
[f] Hepatocellular carcinoma.
[g] Selectivity index.
[h] Control drugs: CQ as diphosphate; MFQ as HCl salt (number of replicates given in parentheses).

## 3. Results and Discussion

Compound **3** was tested *in vitro* for its antiplasmodial activity against three *P. falciparum* strains: D6 (CQ susceptible (CQS) strain), W2 (CQ resistant (CQR) strain), and TM91C235 (Thailand, a multidrug-resistant (MDR) strain). Full method details were previously described [28]. CQ and mefloquine (MFQ) were used as positive controls (Table 1).

As can be seen from Table 1, compound **3** is more active than CQ against CQR W2 strain and MDR TM91C235 strain, and as active as CQ against CQS D6 strain. In addition, it is more active against CQS D6 strain than MFQ.

### 3.1. Fluorescence Spectra and Quenching Mechanism

As it is shown in the literature, the HSA—CQ interactions were studied by different techniques. Results obtained by affinity chromatography, CD and UV–Vis spectroscopy showed no sign of binding [35]. The other study by fluorescence spectroscopy, CD, and UV–Vis spectroscopy gave Stern–Volmer quenching ($K_{SV}$) constant around $1.7 \times 10^4$ at 298 K [36].

Data published so far show the diversity in HSA—CQ binding parameters. Thus we used fluorescence spectroscopy and molecular modeling to study this interaction, as well as the interaction between HSA and 8 representative compounds from different classes of antimalarials synthesized and studied within our research group (compounds **1–8**, Fig. 2). Changes in fluorescence spectrum of HSA upon addition of increasing amounts of CQ diphosphate and compounds **1–8** are shown in Figs. 3 and 4 and in Supplementary material (SM, Figs. S3–S11).

A significant decrease of HSA fluorescence intensity is, among all studied compounds, observed only for **1**, **2**, and **3** (Fig. 4). A slight shift of Trp214 emission maximum (~340 nm) toward lower wavelengths (a blue shift) is observed. Other studied compounds quenched HSA fluorescence in lesser extent (SM, Figs. S7-S11).

The change in the emission maximum wavelength indicates the formation of a complex between HSA and compound, which creates more hydrophobic microenvironment around Trp214.

In order to obtain accurate binding data from spectrofluorimetric measurements, instrumental inner filter effect [37] must be taken into account. Fluorescence intensities can be corrected according to the Lakowicz Eq. (1) by measuring absorbancies at the excitation and emission wavelengths [38]:

$$F_{corr} = F_{obs} \times 10^{\frac{A_{ex}+A_{em}}{2}} \quad (1)$$

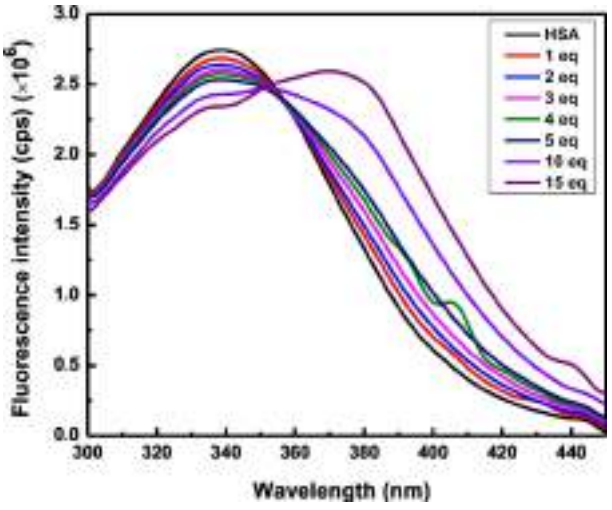


**Fig. 3.** Changes in HSA ($c = 1 \times 10^{-6}$ M) fluorescence emission spectra upon addition of CQ·2$H_3PO_4$ (1–15 mol equivalents) at 298 K, 30 mM PBS, pH = 7.40.

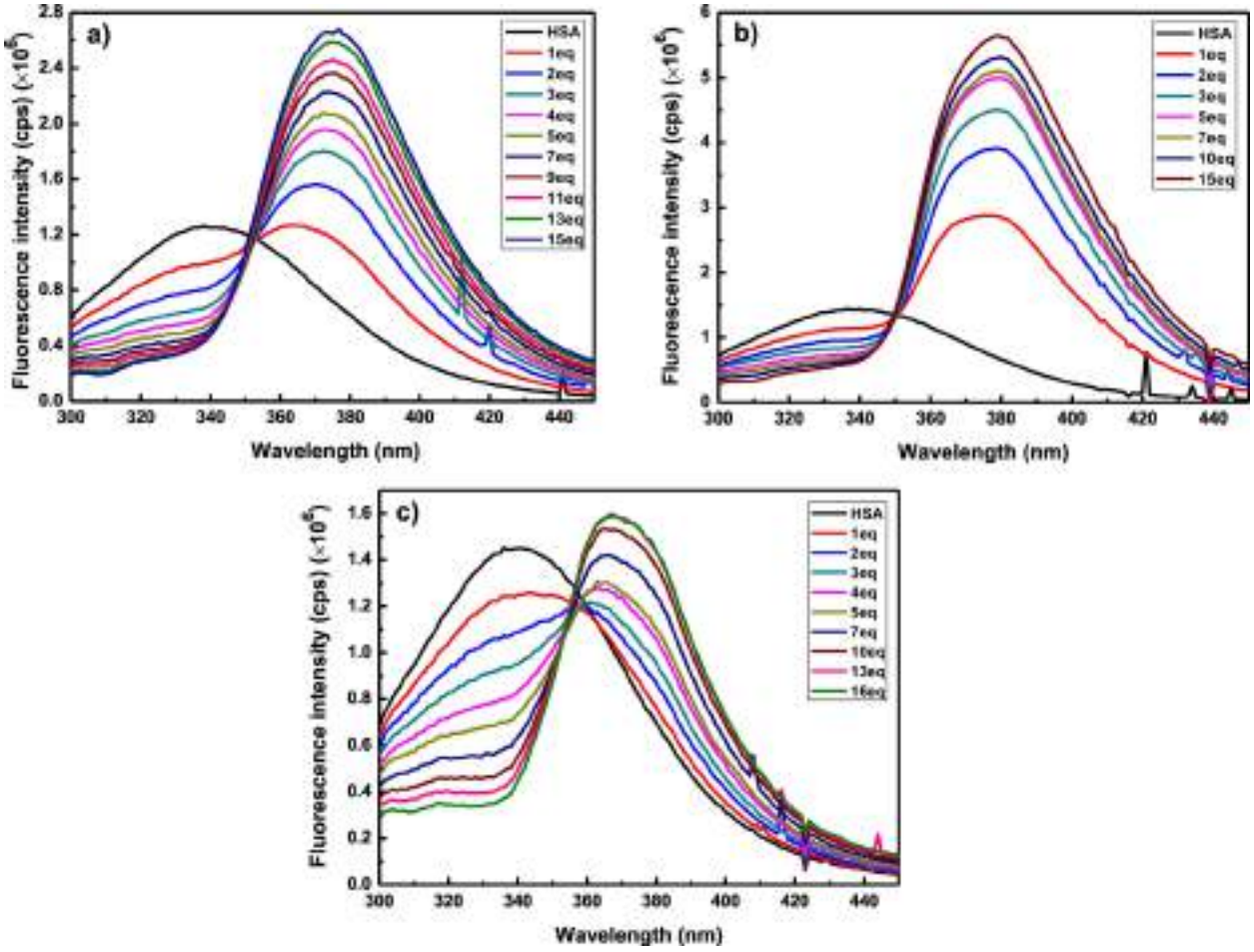


**Fig. 4.** Changes in HSA ($c = 5 \times 10^{-7}$ M) fluorescence emission spectra upon addition of: a) **1,** b) **2**, and c) **3**, in growing concentrations indicated on the graphs; $T = 298$ K, 30 mM PBS, pH = 7.40.

where $F_{corr}$ and $F_{obs}$ stand for corrected and observed fluorescence intensities, and $A_{ex}$ and $A_{em}$ stand for absorbancies at the excitation and emission wavelengths, respectively (UV–Vis spectra are shown on Fig. S12). When the absorbance is lower than 0.07 at both, emission and excitation wavelength, inner filter effect is negligible and such correction can be omitted [39].

Fluorescence quenching data can be processed using Stern-Volmer Eq. (2):

$$\frac{F_0}{F} = 1 + K_{sv}[Q] = 1 + K_q \tau_0 [Q] \quad (2)$$

where $F_0$ and $F$ stand for HSA fluorescence intensities in absence ($F_0$) and in presence of the quencher ($F$), $K_{sv}$ and $K_q$ stand for Stern-Volmer quenching constant and the quenching rate constant of protein, respectively, $\tau_0$ is the average fluorescence lifetime (7.09 ns for HSA) [40], and [Q] is the concentration of the quencher.

All studied compounds showed strong fluorescence emission peak at λ~380 nm when excited with λ = 280 nm (SM, Figs. S3–S11). This peak originates from unbound fraction of compounds. With the increasing compound concentration, emission peak overlaps with the Trp214 emission peak in some extent. In cases of significant overlap (as for compounds **1**–**3**, Fig. 4 and SM, Figs. S4–S6), we collected emission intensities of HSA at lower than maximal emission wavelength (λ = $\lambda_{max}$-20 nm) in order to monitor the emission of Trp 214 exclusively. Attempts to use $\lambda_{max}$ of HSA (~340 nm) resulted in highly downwardly curved Stern-Volmer plots for compounds **1**–**3**, as shown for compound **2** (SM, Fig. S13).

The plots of $F_0/F = f([Q])$ for compounds **1**–**3** at three temperatures are shown on Fig. 5 (and for all other compounds on Fig. S14).

As can be seen in Fig. 5, Stern-Volmer plots are not linear within whole studied HSA/compound molar ratio range, although the wavelength used for calculations is 20 nm lower than the HSA emission maximum wavelength. Still, the curvature is much less pronounced than that shown in SM, Fig. S13. For the calculation of binding constants, only points within linear part were used (up to 5 mol. eq.). These data were used without correction for the inner filter effect, since absorbancies at 280 and 340 nm were below 0.07.

Eq. (2) was used to calculate Stern-Volmer quenching constant ($K_{sv}$) values at three temperatures. Results are given in Table 2.

$K_{sv}$ Values are the largest for compounds **1**–**3**, which indicates stronger interactions with HSA.

Concerning the mechanism, fluorescence quenching could be classified as static or dynamic [38]. Dynamic quenching is highly dependent upon diffusion. Higher temperatures result in faster diffusion and hence larger quenching constant values. On the other hand, higher temperatures will typically result in the dissociation of weakly bound complexes, and therefore decrease the quenching constant in the static process.

For compounds **1**, **3**, **4**, and **6**, as well as for **CQ**, $K_{sv}$ values decrease with increasing temperature (Table 2), which is an indication of static quenching mechanism. Another indication of static quenching mechanism is the value of $K_q$, which is for all studied compounds significantly higher than the maximum scatter collision quenching constant value ($2 \times 10^{10}$ $M^{-1}$ $s^{-1}$) [41].

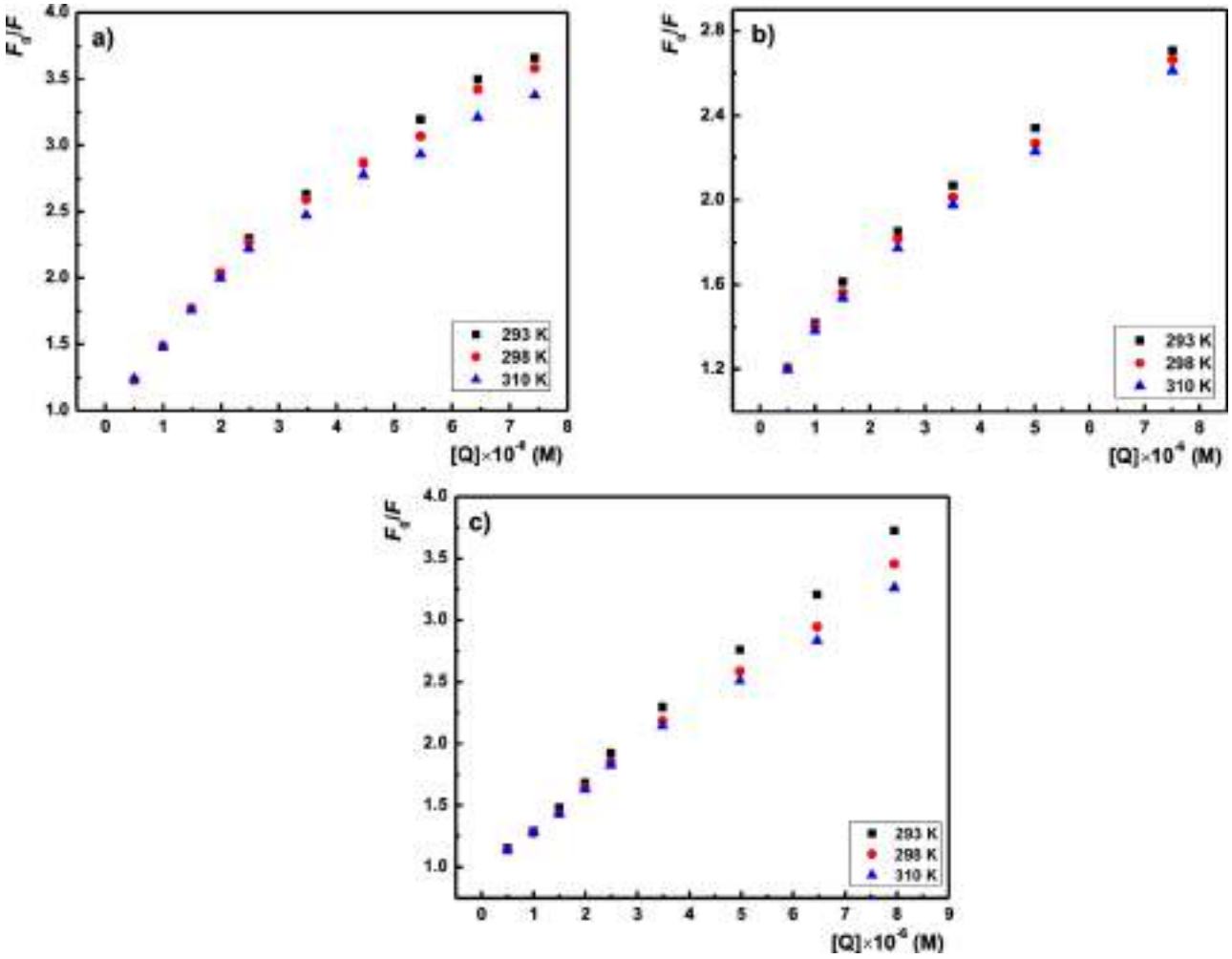


**Fig. 5.** The Stern-Volmer plot for binding of a) **1** (1–15 mol. eq.), b) **2** (1–15 mol. eq.), and c) **3** (1–16 mol. eq.) to HSA ($c = 5 \times 10^{-7}$ M) at 293, 298 and 310 K; pH = 7.40; $\lambda = \lambda_{max}$-20 nm.

Downward curvature in Stern-Volmer plots indicates that the tryptophan residues are not fully accessible to the drug [42]. The fraction of tryptophan residues that are buried and inaccessible to the quencher can be determined by analyzing data using modified Stern-Volmer equation:

$$\frac{F_0}{\Delta F} = \frac{1}{f_a K_a}\frac{1}{[Q]} + \frac{1}{f_a} \quad (3)$$

where $\Delta F$ represent the difference in fluorescence intensity of HSA in the absence ($F_0$) and in the presence of the quencher at concentration [Q]. $K_a$ represents the effective quenching constant for the accessible fluorophores, and $f_a$ is the fraction of the accessible fluorophore. Results are shown on Fig. 6 (and for all other compounds on Fig. S15) and Table 3.

As shown in Table 3, all compounds have similar effective quenching constants, but the fraction of accessible fluorophore was much higher for **1**, **2**, and **3** compared to **CQ** and **4**–**8**. Compounds with lower $K_{sv}$ values also have very low $f_a$s, indicating the low accessibility of Trp214 to weakly bound compounds.

Considering differences in $K_a$ and $K_{sv}$ values shown in Tables 2 and 3 it is good to point out that $K_a$ is actually the Stern-Volmer quenching

**Table 2**
Stern-Volmer quenching constant ($K_{sv}$) and the quenching rate constant of protein ($K_q$) values at three temperatures; the average fluorescence lifetime $\tau_0 = 7.09$ ns. $K_{sv}$ is obtained as a linear regression slope while the intercept was kept constant ($F_0/F = 1$).

| $T$ (K) | 293 | | 298 | | 310 | |
|---|---|---|---|---|---|---|
| Comp. | $(K_{sv} \pm SD) \times 10^5$ ($M^{-1}$) | $K_q \times 10^{13}$ ($M^{-1}$ $s^{-1}$) | $(K_{sv} \pm SD) \times 10^5$ ($M^{-1}$) | $K_q \times 10^{13}$ ($M^{-1}$ $s^{-1}$) | $(K_{sv} \pm SD) \times 10^5$ ($M^{-1}$) | $K_q \times 10^{13}$ ($M^{-1}$ $s^{-1}$) |
| **CQ** | 0.37 ± 0.02 | 0.53 | 0.35 ± 0.01 | 0.49 | 0.27 ± 0.01 | 0.38 |
| **1** | 5.18 ± 0.07 | 7.30 | 5.14 ± 0.05 | 7.25 | 4.97 ± 0.04 | 7.01 |
| **2** | 3.65 ± 0.20 | 5.15 | 3.46 ± 0.17 | 4.88 | 8.92 ± 1.89 | 12.58 |
| **3** | 3.47 ± 0.12 | 4.90 | 3.23 ± 0.11 | 4.55 | 3.16 ± 0.10 | 4.45 |
| **4** | 0.44 ± 0.03 | 0.62 | 0.29 ± 0.04 | 0.41 | /* | /* |
| **5** | 0.24 ± 0.01 | 0.34 | 0.34 ± 0.02 | 0.48 | 0.15 ± 0.01 | 0.21 |
| **6** | 0.85 ± 0.07 | 1.19 | 0.29 ± 0.01 | 0.42 | 0.25 ± 0.03 | 0.35 |
| **7** | 0.73 ± 0.05 | 1.03 | 0.94 ± 0.03 | 1.33 | 0.77 ± 0.03 | 1.09 |
| **8** | 0.52 ± 0.04 | 0.74 | 0.58 ± 0.03 | 0.82 | 0.40 ± 0.04 | 0.56 |

* Emission spectra changes upon addition of quencher were too small, and therefore $K_{sv}$ could not be accurately calculated.

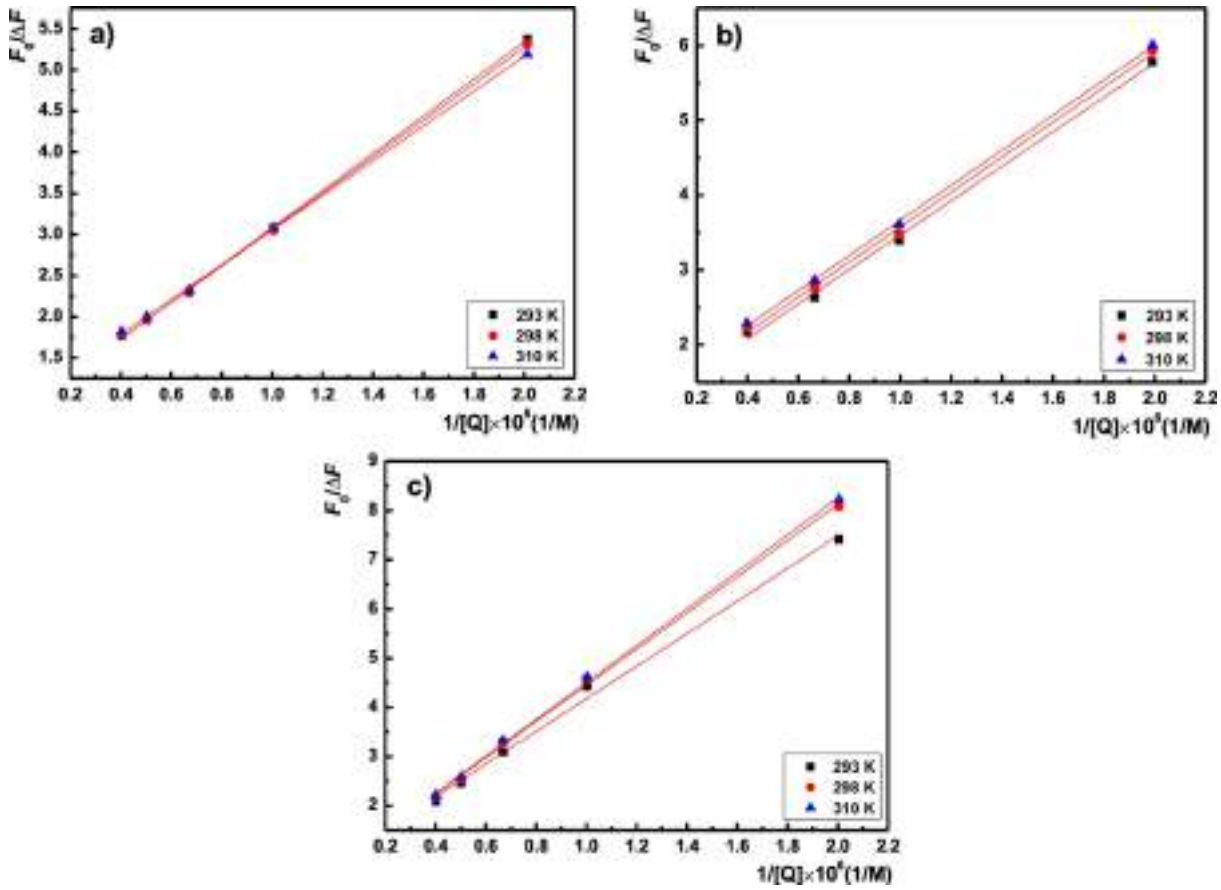


**Fig. 6.** Modified Stern-Volmer plot for binding of a) **1**, b) **2**, and c) **3** to HSA ($c = 5 \times 10^{-7}$ M) in 1–15/16 mol. eq. at 293, 298, and 310 K; pH = 7.40; $\lambda = \lambda_{max}$-20 nm.

constant of the accessible fraction of fluorophore. Compounds **1**–**3** have fraction of accessible fluorophore ($f_a$) close to 1 (Table 3), and their $K_a$ values are in a good accordance with $K_{sv}$ values. For other studied compounds that bind weakly to HSA (CQ and **4**–**8**), $K_{sv}$ values are approximately one order of magnitude lower than $K_{sv}$ values of compounds **1**–**3**. However, the fraction of accessible fluorophore for these compounds is only 0.1–0.2; the effective quenching constant, $K_a$, has similar or even higher values than for compounds **1**–**3**. Total quenching constant, $K_{sv}$, equals the effective quenching constant ($K_a$) multiplied by the fraction of accessible fluorophore ($f_a$): $K_{sv} = K_a \times f_a$.

From the molecular standpoint of view, lower binding constants of **4**–**8** compared to **1**–**3** could be due to inability of compounds **4**–**8** to approach Trp214 and accept the energy when Trp214 is in the excited state. We assume that Trp214 is just partially accessible to compounds **4**–**8**.

For the majority of compounds, Trp214 is less accessible to quencher with increasing the temperature, so we may conclude that it becomes more buried inside the hydrophobic interior of protein at higher temperatures. Also, $\lambda_{max}$ of HSA emission shows blue shift as temperature increases from 293 to 310 K. The emission from an exposed surface Trp residue will occur at longer wavelengths than that from a Trp residue in the protein's interior [38].

**Table 3**
Modified Stern-Volmer effective quenching constant at three temperatures.

| $T$ (K) | 293 | | 298 | | 310 | |
|---|---|---|---|---|---|---|
| Comp. | $(K_a \pm SD) \times 10^5$ ($M^{-1}$) | $f_a$ | $(K_a \pm SD) \times 10^5$ ($M^{-1}$) | $f_a$ | $(K_a \pm SD) \times 10^5$ ($M^{-1}$) | $f_a$ |
| **CQ** | 3.62 ± 0.36 | 0.162 | 2.51 ± 0.13 | 0.192 | 4.97 ± 0.70 | 0.099 |
| **1** | 3.65 ± 0.13 | 1.214 | 3.84 ± 0.16 | 1.179 | 4.47 ± 0.12 | 1.061 |
| **2** | 5.05 ± 0.44 | 0.860 | 5.26 ± 0.35 | 0.812 | 5.61 ± 0.21 | 0.760 |
| **3** | 2.61 ± 0.43 | 1.156 | 2.11 ± 0.26 | 1.288 | 2.04 ± 0.18 | 1.312 |
| **4** | 7.88 ± 1.08 | 0.126 | 14.8 ± 1.34 | 0.071 | /* | /* |
| **5** | 3.43 ± 0.50 | 0.109 | 4.04 ± 0.28 | 0.140 | 4.53 ± 0.58 | 0.061 |
| **6** | 9.24 ± 1.28 | 0.216 | 3.30 ± 0.53 | 0.139 | 13.60 ± 1.24 | 0.063 |
| **7** | 7.83 ± 1.55 | 0.198 | 3.79 ± 0.24 | 0.361 | 3.66 ± 0.14 | 0.314 |
| **8** | 8.19 ± 0.86 | 0.148 | 4.45 ± 0.15 | 0.218 | 7.28 ± 0.20 | 0.111 |

* Emission spectra changes upon addition of quencher were too small, and therefore $K_a$ could not be accurately calculated.

### 3.2. Analysis of Binding Equilibria – Binding Constant and the Number of Binding Sites

When small molecules bind independently to a set of equivalent sites of the protein, the equilibrium between free and bound molecules for the static quenching process is given by the Eq. (4):

$$\log\frac{F_0 - F}{F} = \log K_b + n \log[Q] \quad (4)$$

where $F_0$ and $F$ have the same meaning as in previous equations; $K_b$ is equilibrium binding constant, and $n$ is the number of binding sites. Linear dependence for HSA – compounds **1**–**3** binding is shown on Fig. 7 (and for all other compounds on Fig. S16); the results of linear regression analysis are given in Table 4.

Compounds **1**–**3** have higher $\log K_b$ values than **CQ** and the rest of compounds, again indicating stronger binding interactions. For compounds with higher $\log K_b$ values (**1**–**3**), a number of binding sites is approximately 1.

Obtained binding constant values for **1**–**3** indicate that these compounds can be effectively transported bound to HSA to the site of

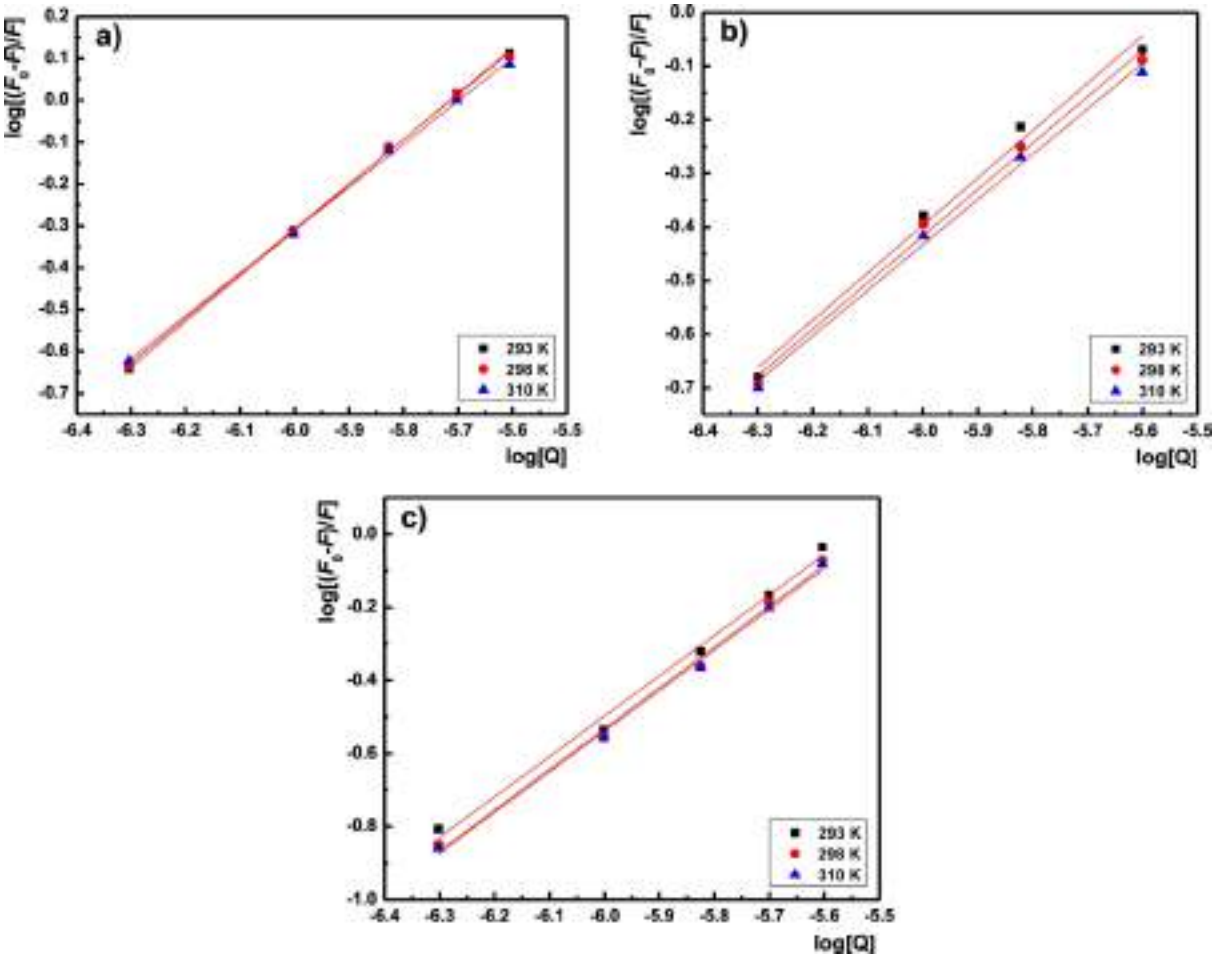


**Fig. 7.** Log-log plot for the determination of binding constants $K_b$, and the number of binding sites $n$ for binding of a) **1**, b) **2**, and c) **3** (1–5 mol. eq.) to HSA ($c = 5 \times 10^{-7}$ M) at three temperatures.

biological action in the human organism. The consumption of molecule at the site of action would shift the equilibrium toward releasing of new amount of compound from compound/HSA complex.

### 3.3. Displacement Experiments

In order to determine the binding site on HSA, we recorded fluorescence spectra of complex HSA–Wf/Dz upon addition of compounds **1**–**3** (fluorescent emission spectra along with corresponding log-log plots are given in Supplementary material (Figs. S17–S19)). Calculated equilibrium binding constants for the displacement reactions are shown in Table 5.

**Table 4**
Binding constants and the number of binding sites at three temperatures.

| $T$ (K) | 293 | | 298 | | 310 | |
|---|---|---|---|---|---|---|
| Comp. | log$K_b$ ± SD | $n$ | log$K_b$ ± SD | $n$ | log$K_b$ ± SD | $n$ |
| **CQ** | 3.21 ± 0.12 | 0.762 | 3.48 ± 0.11 | 0.815 | 2.72 ± 0.24 | 0.702 |
| **1** | 6.22 ± 0.07 | 1.088 | **6.10 ± 0.10** | **1.068** | 5.84 ± 0.09 | 1.026 |
| **2** | 4.91 ± 0.37 | 0.885 | **4.79 ± 0.29** | **0.868** | 4.64 ± 0.24 | 0.846 |
| **3** | 6.13 ± 0.32 | 1.104 | **6.17 ± 0.27** | **1.116** | 6.12 ± 0.22 | 1.110 |
| **4** | 2.36 ± 0.13 | 0.601 | 1.05 ± 0.25 | 0.404 | /* | /* |
| **5** | 3.10 ± 0.13 | 0.776 | 2.94 ± 0.15 | 0.722 | 2.19 ± 0.43 | 0.654 |
| **6** | 2.57 ± 0.17 | 0.588 | 3.06 ± 0.28 | 0.754 | 1.05 ± 0.28 | 0.416 |
| **7** | 2.82 ± 0.28 | 0.644 | 3.83 ± 0.05 | 0.800 | 3.64 ± 0.13 | 0.781 |
| **8** | 2.36 ± 0.15 | 0.588 | 3.19 ± 0.09 | 0.725 | 2.33 ± 0.23 | 0.608 |

* Emission spectra changes upon addition of quencher were too small, and therefore $K_b$ could not be accurately calculated.

Binding constants shown in Table 5 compared to binding constants for HSA–compound **1**–**3** interaction at 298 K (given in Table 4 and shown in bold) indicate that compounds **1**–**3** bind significantly stronger to warfarin binding site (site I) compared to diazepam binding site (site II).

### 3.4. Thermodynamic Parameters of Binding

If the equilibrium binding constant of ligand to protein reaction is measured at several temperatures, the enthalpy ($\Delta H$) and entropy change ($\Delta S$) during the process can be determined according to Van't Hoff Eq. (5):

$$\ln K_a = -\frac{\Delta H}{RT} + \frac{\Delta S}{R} \tag{5}$$

**Table 5**
Binding constants and the number of binding sites for competitive reaction HSA–comp + Wf/Dz at 298 K.

| Compound | Site specific probe | | | |
|---|---|---|---|---|
| | Warfarin | | Diazepam | |
| | log$K_b$ ± SD | $n$ | log$K_b$ ± SD | $n$ |
| **1** | 5.01 ± 0.03 | 0.958 | 5.62 ± 0.05 | 1.053 |
| **2** | 4.11 ± 0.05 | 0.786 | 4.93 ± 0.05 | 0.954 |
| **3** | 5.44 ± 0.10 | 1.081 | 6.26 ± 0.17 | 1.253 |

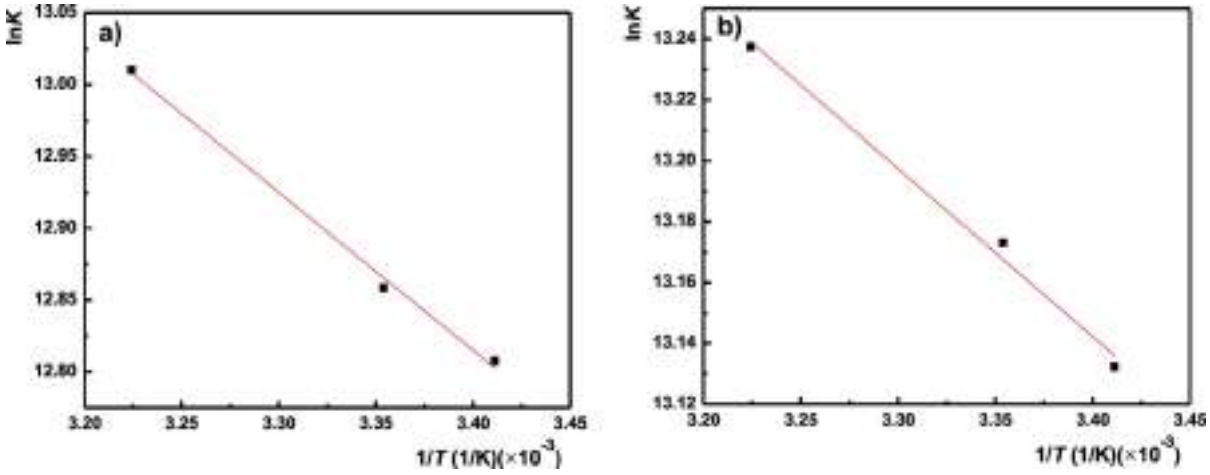


**Fig. 8.** The plot of ln$K_a$ *vs.* 1/T for the interaction of a) **1** and b) **2** with HSA.

where $R$ is the universal gas constant, $T$ is the temperature (in K), and $K_a$ is the effective quenching constant at the corresponding temperature. Results for binding of **1** and **2** to HSA, are shown in Fig. 8.

Thermodynamic parameters for compounds **1** and **2** binding to HSA are summarized in Table 6. Attempts to plot ln$K_a$ *vs.* $1/T$ for compound **3** resulted in the line with the positive slope and poor correlation coefficient, so these data are omitted.

According to Ross' view [43], the signs and magnitudes of thermodynamic parameters for protein reactions can account for the main forces contributing to protein stability. From the thermodynamic standpoint, $\Delta H > 0$ and $\Delta S > 0$ implies a hydrophobic interaction, $\Delta H < 0$ and $\Delta S < 0$ reflects the van der Waals force or hydrogen bond formation and $\Delta H < 0$ and $\Delta S > 0$ suggesting an electrostatic force.

The positive values of enthalpy and entropy changes indicate that the hydrophobic interactions are the main contributors to HSA–**1** and HSA–**2** binding. For compound **1**, $T\Delta S$ term is ~4 times higher than $\Delta H$, while this ratio is ~8 for compound **2**. For both compounds, entropic term ($T\Delta S$) dominates over enthalpic ($\Delta H$), pointing on nonspecific binding interactions as the main contributors to the overall binding energy.

### 3.5. Molecular Docking and Lipophilicity Descriptors

To elucidate binding of investigated compounds to HSA, a series of molecular docking experiments was performed. Close examination of best scored binding poses showed similarities in binding positions for investigated ligands (Fig. 9).

Chloroquine/quinoline part of the molecule resides outside of standard warfarin binding site (Site I, Fig. 1), interacting with Glu153 and Glu252 by a salt bridge and H-bonding to side chain, respectively. This part of the protein is largely exposed to solvent and plays role in stabilization of HSA conformation. Protonated secondary nitrogen residing in alkyl bridge is, to some extent, exposed to solvent, which can be very significant in unbinding the ligand from HSA and low values of binding constants. This part of the molecule is, more or less, similar in all examined molecules. Binding positions for this part of the molecule are similar as well.

Second part of the molecule resides in the position of 4-hydroxy-2*H*-chromen-2-one part of warfarin molecule. Since these groups lack the ability to form hydrogen bonds or their hydrogen bond capable parts are not correctly oriented, contrary to warfarin molecule, this part of the molecule is stabilized with hydrophobic interactions dominantly, residing in a hydrophobic pocket formed by following amino acid residues: Phe211, Trp214, Leu219, Leu238, Leu260, Ala261, Ile290, Ala291. These residues generally form well known IIA binding site of HSA [44]. Aromatic moiety of **1**–**6** also binds to aromatic residues His242 and Arg257 by π-π and cation-π interactions.

Since only sulphur-containing compounds (**1**–**3**) are strongly bound to HSA, one may suppose that additional S-π (or π-π) interactions stabilize HSA–compound complex. Due to the lack of such feature, those interaction(s) are not observed in molecular docking calculations, as shown in ligand interaction diagram (Fig. 10). However, the interaction between sulphur atoms and aromatic residues has been reported to be important for the stabilization of protein structure [45–47]. Therefore, we can assume that similar, additional stabilization is noticed here as well, but additional theoretical studies are needed for further conclusions.

From ligand interaction diagram we can conclude that all of the investigated compounds can share the same set of interactions in aminoquinoline part of the molecule: π-cation interaction with Lys195, electrostatic interaction with Glu153 and H-bond with Glu292 side chain. Also, there is a small hydrophobic pocket made by Phe157 and Ala191 and polar interaction between Ser192 and nitrogen directly connected to aromatic ring. The compounds with aromatic moiety on the other part of the molecule, like thiophene ring, can also form π-stacking interactions with Arg257 and His242. However, the most polar group, protonated aliphatic nitrogen, stays exposed to the solvent and probably can be used as an "extraction handle" for unbinding the compound from HSA.

With the exception of acidic compounds (negatively charged at physiological pH), binding constants of drugs to HSA are well correlated with their lipophilicity [3]. In order to test whether this hypothesis may explain obtained results, we calculated several lipophilicity descriptors (Table 7).

The paired $t$-test shows that the average values of descriptors for compounds that bind to HSA more strongly (**1**–**3**) and weakly binding compounds (**4**–**8** and **CQ**) are significantly different. Increased

**Table 6**
Docking scores, MM-GBSA binding energies and thermodynamic parameters of compounds **1** and **2** binding to HSA calculated according to Van't Hoff Eq. (5), $T = 298$ K.

| Compound | Docking score (kJmol$^{-1}$) | MM-GBSA dG Bind (NS) energy (kJmol$^{-1}$) | $\Delta H°$ (kJ/mol) | $\Delta G°$ (kJ/mol) | $\Delta S°$ (Jmol$^{-1}$ K$^{-1}$) | $T\Delta S°$ (kJmol$^{-1}$) |
|---|---|---|---|---|---|---|
| **1** | −13.38 | −310.26 | 9.13 | −31.87 | 137.60 | 41.03 |
| **2** | −14.42 | −313.00 | 4.58 | −32.65 | 124.84 | 37.22 |

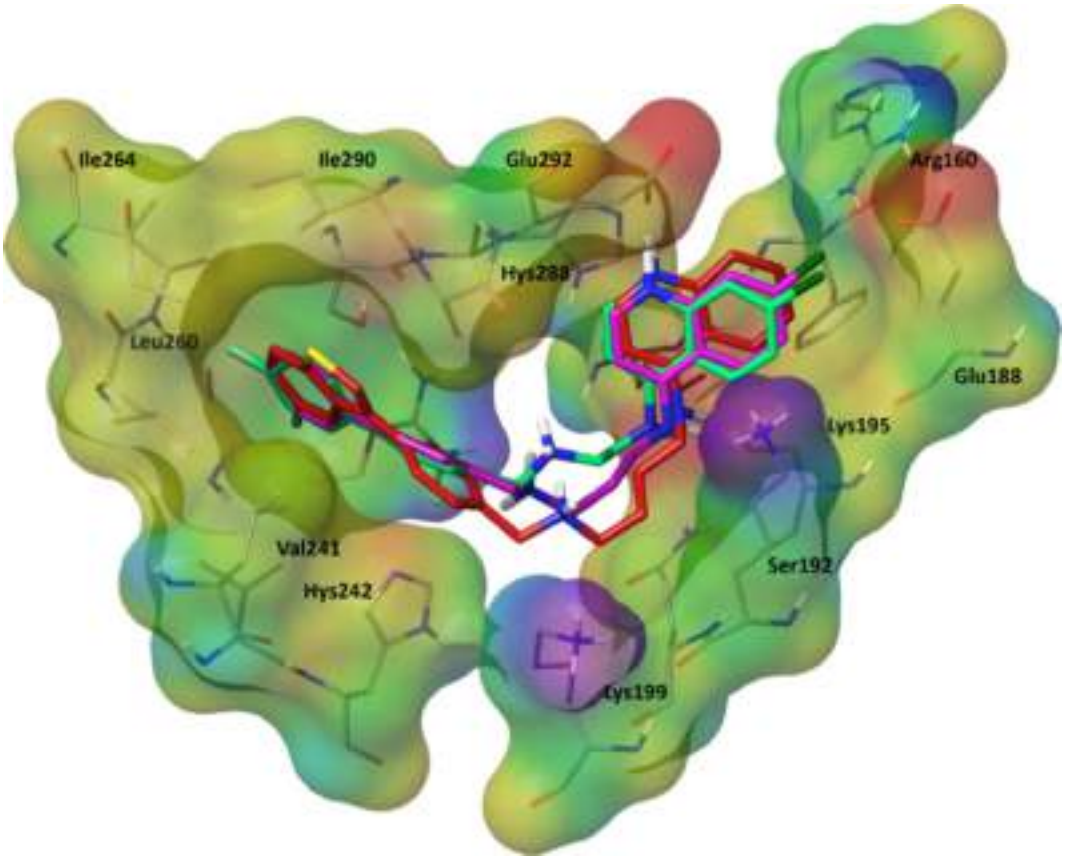


**Fig. 9.** The binding pose of compounds **1** (green), **2** (pink) and **3** (red) into HSA. (For interpretation of the references to colour in this figure legend, the reader is referred to the web version of this article.)

lipophilicity of sulphur-containing compounds might be a reason for better HSA binding. It points on the non-specific, hydrophobic forces as the most important ones for binding of these compounds to HSA. The same findings are derived using Van't Hoff equation.

## 4. Conclusions

Interactions between human serum albumin (HSA) and eight in-house synthesized aminoquinolines (**1**–**8**), potent antimalarials,

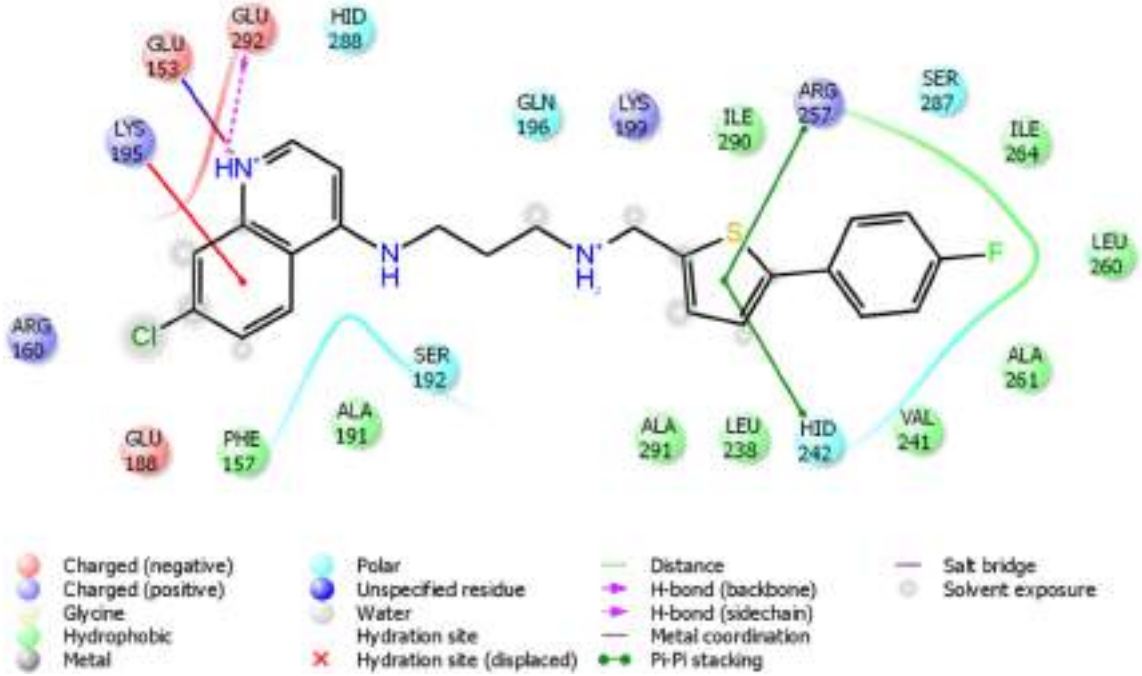


**Fig. 10.** Ligand interaction diagram for compound **2**.

**Table 7**
Calculated lipophilicity descriptor values. Average values of each descriptor are shown as <**sb**> for stronger bound (**1**–**3**) and <**wb**> for weakly bound (**4**–**8** and **CQ**) compounds.

| Comp. | | | | | | | | | | | |
|---|---|---|---|---|---|---|---|---|---|---|---|
| Descr. | **1** | **2** | **3** | <**sb**> | **4** | **5** | **6** | **7** | **8** | **CQ** | <**wb**> |
| log*P* (Crippen) | 4.700 | 5.229 | 6.003 | 5.310 | 3.567 | 4.096 | 3.938 | NP* | 6.067 | 4.320 | 4.398 |
| Lipole (Crippen) | 3.163 | 2.858 | 2.004 | 2.675 | 1.911 | 2.255 | 2.139 | NP* | 1.010 | 1.431 | 1.749 |
| log*P* (Broto) | 7.443 | 7.897 | 8.808 | 8.049 | 4.883 | 5.337 | 5.086 | 5.953 | 7.356 | 4.741 | 5.559 |
| Lipole (Broto) | 3.751 | 3.598 | 4.235 | 3.861 | 2.087 | 2.463 | 2.329 | 2.102 | 1.589 | 2.755 | 2.221 |
| Virtual log*P* | 6.275 | 6.906 | 8.343 | 7.175 | 5.171 | 5.279 | 4.999 | 6.121 | 6.781 | 5.389 | 5.623 |

* NP: no parameters for calculation were found.

along with well-known chloroquine (**CQ**), have been studied in phosphate buffered saline (pH 7.40) by fluorescence spectroscopy. Results show that three compounds having additional thiophene or benzothiophene substructure (**1**–**3**, Fig. 2) bind more strongly to HSA than other studied compounds. Fluorescence quenching at three temperatures (20, 25, and 37 °C) was analyzed using classical Stern-Volmer equation, and a static quenching mechanism was proposed. As shown in Table 3, all compounds have similar effective quenching constants, but the fraction of accessible fluorophore was much higher for **1**, **2**, and **3** compared to **CQ** and **4**–**8**. For the majority of studied compounds, Trp214 is less accessible to quencher with increasing the temperature. It is thus concluded that it becomes more buried inside the hydrophobic interior of the protein at higher temperatures.

Effective quenching constants of compounds **1**–**3** are in the order of $10^5$ $M^{-1}$ (Table 3), meaning that these compounds can be effectively carried and stored by HSA in the human body. Binding constants (log$K_b$) were also calculated (Table 4). Compounds **1**–**3** have higher log$K_b$ values (4.91–6.22, at 20 °C) than **CQ** and the rest of compounds (log$K_b$ 2.36–3.21, at 20 °C), again indicating stronger binding interactions. For compounds with higher log$K_b$ values (**1**–**3**), a number of binding sites is approximately 1. Competitive binding experiments showed that compounds **1**–**3** bind significantly stronger to warfarin (site I) compared to diazepam binding site (site II).

The enthalpy and entropy changes upon HSA–sulphur-containing compound interactions were calculated using Van't Hoff equation. Positive values of enthalpy and entropy changes, as well as higher impact of entropic term ($T\Delta S$) compared to enthalpic ($\Delta H$) point to the non-specific, hydrophobic interactions as the main contributors to HSA–compound interaction.

To elucidate binding of investigated compounds to HSA, a series of molecular docking experiments was performed. Since only sulphur-containing compounds (**1**–**3**) are strongly bound to HSA, one may suppose that additional S-π (or π-π) interactions stabilize HSA–compound complex. Due to the lack of such feature, those interaction(s) are not observed in molecular docking calculations, as shown in ligand interaction diagram (Fig. 10).

Calculated lipophilicity descriptor values, along with molecular docking studies, point out that the increased lipophilicity of sulphur-containing compounds might be a reason for their better binding to HSA.

Obtained results might contribute to design of novel aminoquinoline derivatives with improved pharmacokinetic properties and drug efficacy.

## Acknowledgements

This work was supported by the Ministry of Education, Science, and Technological Development of Serbia [grant numbers 172008, 172035]; Serbian Academy of Sciences and Arts [grant number F80]; and the European Commission – FP7 RegPot project FCUB ERA GA [grant number 256716].

## Appendix A. Supplementary data

Supplementary data to this article can be found online at https://doi.org/10.1016/j.saa.2017.10.061.

## References

[1] T. Peters Jr., All About Albumin, Biochemistry, Genetics, and Medical Applications, First ed. AcademicPress, San Diego, California, USA, 1995.
[2] M.A.K. Azad, J.X. Huang, M.A. Cooper, K.D. Roberts, P.E. Thompson, R.L. Nation, J. Li, T. Velkov, Structure–activity relationships for the binding of polymyxins with human a-1-acid glycoprotein, Biochem. Pharmacol. 84 (2012) 278–291.
[3] K. Valko, S. Nunhuck, C. Bevan, M.H. Abraham, D.P. Reynolds, Fast gradient HPLC method to determine compounds binding to human serum albumin. Relationships with octanol/water and immobilized artificial membrane lipophilicity, J. Pharm. Sci. 92 (2003) 2236–2248.
[4] E.F. Pettersen, T.D. Goddard, C.C. Huang, G.S. Couch, D.M. Greenblatt, E.C. Meng, T.E. Ferrin, UCSF Chimera—A visualization system for exploratory research and analysis, J. Comput. Chem. 25 (2004) 1605–1612.
[5] K. Yamasaki, V.T.G. Chuang, T. Maruyama, M. Otagiri, Albumin-drug interaction and its clinical implication, Biochim. Biophys. Acta Gen. Subj. 1830 (2013) 5435–5443.
[6] J. Ghuman, P.A. Zunszain, I. Petitpas, A.A. Bhattacharya, M. Otagiri, S. Curry, Structural basis of the drug-binding specificity of human serum albumin, J. Mol. Biol. 353 (2005) 38–52.
[7] T. Bohnert, L.-S. Gan, Plasma protein binding: from discovery to development, J. Pharm. Sci. 102 (9) (2013) 2953–2994.
[8] R. Punith, A.H. Hegde, S. Jaldappagari, Binding of an anti-inflammatory drug lornoxicam with blood proteins: insights from spectroscopic investigations, J. Fluoresc. 21 (2011) 487–495.
[9] Y.S. Wang, D. Liu, D.F. Wyss, S.T.D.N.M.R. Competition, For the detection of high-affinity ligands and NMR-based screening, Magn. Reson. Chem. 42 (2004) 485–489.
[10] L.V. Elst, F. Chapelle, S. Laurent, R.N. Muller, Stereospecific binding of MRI contrast agents to human serum albumin: the case of Gd-(S)-EOB-DTPA (Eovist) and its (R) isomer, J. Biol. Inorg. Chem. 6 (2001) 196–200.
[11] B. Meyer, T. Peters, NMR spectroscopy techniques for screening and identifying ligand binding to protein receptors, Angew. Chem. Int. Ed. 42 (2003) 864–890.
[12] C. Ràfols, S. Zarza, E. Bosch, Molecular interactions between some non-steroidal anti-inflammatory drugs (NSAID's) and bovine (BSA) or human (HSA) serum albumin estimated by means of isothermal titration calorimetry (ITC) and frontal analysis capillary electrophoresis (FA/CE), Talanta 130 (2014) 241–250.
[13] H. Aki, M. Yamamoto, Thermodynamic characterization of drug binding to human serum albumin by isothermal titration microcalorimetry, J. Pharm. Sci. 83 (1994) 1712–1716.
[14] Y. Sun, Z. Ji, X. Liang, G. Li, S. Yang, S. Wei, Y. Zhao, X. Hu, Jun fan, studies on the binding of rhaponticin with human serum albumin by molecular spectroscopy, modeling and equilibrium dialysis, Spectrochim. Acta A 87 (2012) 171–178.
[15] K.S. Joseph, D.S. Hage, Characterization of the binding of sulfonylurea drugs to HSA by high-performance affinity chromatography, J. Chromatogr. B 878 (2010) 1590–1598.
[16] L.V. Elst, F. Chapelle, S. Laurent, R.N. Muller, Comprehensive investigation of the non-covalent binding of MRI contrast agents with human serum albumin, J. Biol. Inorg. Chem. 12 (2007) 929–937.
[17] S. Neamtu, N. Tosa, M. Bogdan, Spectroscopic investigation of tolmetin interaction with human serum albumin, J. Pharm. Biomed. 85 (2013) 277–282.
[18] Í.P. Caruso, W. Vilegas, F. Perreira de Souza, M.A. Fossey, M.L. Cornélio, Binding of antioxidant flavone isovitexin to human serum albumin investigated by experimental and computational assays, J. Pharm. Biomed. 98 (2014) 100–106.
[19] J. Liu, Y. Yue, J. Wang, X. Yan, R. Liu, Y. Sun, X. Li, Study of interaction between human serum albumin and three phenanthridine derivatives: fluorescence spectroscopy and computational approach, Spectrochim. Acta A 145 (2015) 473–481.
[20] Y. Yue, J. Liu, R. Liu, Q. Dong, J. Fan, Binding of helicid to human serum albumin: a hybrid spectroscopic approach and conformational study, Spectrochim. Acta A 124 (2014) 46–51.
[21] Y. Yue, Q. Dong, Y. Zhang, X. Li, X. Yan, Y. Sun, J. Liu, Synthesis of imidazole derivatives and the spectral characterization of the binding properties towards human serum albumin, Spectrochim. Acta A 153 (2016) 688–703.

[22] F. Cuia, Y. Yana, Q. Zhanga, X. Yaob, G. Qua, Y. Lua, Characterization of the interaction between 8-bromoadenosine with human serum albumin and its analytical application, Spectrochim. Acta A 74 (2009) 964–971.
[23] Md. Mushtaque, Shahjahan, Reemergence of chloroquine (CQ) analogs as multi-targeting antimalarial agents: A review, Eur. J. Med. Chem. 90 (2015) 280–295.
[24] I.M. Opsenica, T.Ž. Verbić, M. Tot, R.J. Sciotti, B.S. Pybus, O. Djurković-Djaković, K. Slavić, B.A. Šolaja, Investigation into novel thiophene- and furan-based 4-amino-7-chloroquinolines afforded antimalarials that cure mice, Bioorg. Med. Chem. 23 (2015) 2176–2186.
[25] I.M. Opsenica, M. Tot, L. Gomba, J.E. Nuss, R.J. Sciotti, S. Bavari, J.C. Burnett, B.A. Šolaja, 4-amino-7-chloroquinolines: probing ligand efficiency provides botulinum neurotoxin serotype a light chain inhibitors with significant antiprotozoal activity, J. Med. Chem. 56 (2013) 5860–5871.
[26] I. Opsenica, D. Opsenica, C.A. Lanteri, L. Anova, W.K. Milhous, K.S. Smith, B.A. Šolaja, New chimeric antimalarials with 4-aminoquinoline moiety linked to a tetraoxane skeleton, J. Med. Chem. 51 (2008) 6216–6219.
[27] N. Terzić, J. Konstantinović, M. Tot, J. Burojević, O. Djurković-Djaković, J. Srbljanović, T. Štajner, T. Verbić, M. Zlatović, M. Machado, I.S. Albuquerque, M. Prudêncio, R.J. Sciotti, S. Pecic, S. D'Alessandro, D. Taramelli, B.A. Šolaja, Reinvestigating old pharmacophores: are 4-aminoquinolines and tetraoxanes potential two-stage antimalarials? J. Med. Chem. 59 (2016) 264–281.
[28] J. Konstantinović, M. Videnović, J. Srbljanović, O. Djurković-Djaković, K. Bogojević, R. Sciotti, B. Šolaja, Antimalarials with benzothiophene moieties as aminoquinoline partners, Molecules 22 (3) (2017) 343.
[29] I. Petitpas, A.A. Bhattacharya, S. Twine, M. East, S. Curry, Crystal structure analysis of warfarin binding to human serum albumin: anatomy of drug site I, J. Biol. Chem. 276 (25) (2001) 22804–22809.
[30] J.L. Knight, G. Krilov, K.W. Borrelli, J. Williams, J.R. Gunn, A. Clowes, L. Cheng, R.A. Friesner, R. Abel, Leveraging data fusion strategies in multireceptor lead optimization MM/GBSA end-point methods, J. Chem. Theory Comput. 10 (2014) 3207–3220.
[31] P.C.D. Hawkins, A. Nicholls, Conformer generation with OMEGA: learning from the data set and the analysis of failures, J. Chem. Inf. Model. 52 (2012) 2919–2936 (OMEGA v. 2.5.1.4, OpenEye scientific software, Santa Fe, NM. http://www.eyesopen.com (accessed 04.05.17)).
[32] J.J.P. Stewart, MOPAC: A semiempirical molecular orbital program, J. Comput. Aided Mol. Des. 4 (1) (1990) 1–103 (MOPAC2016; Stewart Computational Chemistry, Colorado Springs, CO, USA. http://OpenMOPAC.net (accessed 04.05.17)).
[33] J.J.P. Stewart, Optimization of parameters for semiempirical methods V: modification of NDDO approximations and application to 70 elements, J. Mol. Model. 13 (2007) 1173–1213.
[34] A. Pedretti, L. Villa, G. Vistoli, VEGA—an open platform to develop chemo-bio-informatics applications, using plug-in architecture and script programming, J. Comput. Aided Mol. Des. 18 (3) (2004) 167–173 (VegaZZ 3.0.3. http://www.ddl.unimi.it (accessed 04.05.17)).
[35] F. Zsila, J. Visy, G. Mády, I. Fitos, Selective plasma protein binding of antimalarial drugs to α1-acid glycoprotein, Bioorg. Med. Chem. 16 (2008) 3759–3772.
[36] S. Tunç, O. Duman, B.K. Bozoğlan, Studies on the interactions of chloroquinediphosphate and phenelzine sulfate drugs with human serum albumin and human hemoglobin proteins by spectroscopic techniques, J. Lumin. 140 (2013) 87–94.
[37] B. Birdsall, R.W. King, M.R. Wheeler, C.A. Lewis Jr., S.R. Goode, R.B. Dunlap, G.C. Roberts, Correction for light absorption in fluorescence studies of protein-ligand interactions, Anal. Biochem. 132 (1983) 353–361.
[38] J.R. Lakowicz, Principles of Fluorescence Spectroscopy, Third ed. Springer Science Business Media, New York, USA, 2006.
[39] N. Seedher, S. Bhatia, Reversible binding of celecoxib and valdecoxib with human serum albumin using fluorescence spectroscopic technique, Pharmacol. Res. 54 (2006) 77–84.
[40] M. Amiri, K. Jankeje, J.R. Albani, Origin of fluorescence lifetimes in human serum albumin. Studies on native and denatured protein, J. Fluoresc. 20 (2010) 651–656.
[41] M.R. Eftink, C.A. Ghiron, Fluorescence quenching studies with proteins, Anal. Biochem. 114 (1981) 199–227.
[42] S.S. Lehrer, Solute perturbation of protein fluorescence. The quenching of the tryptophyl fluorescence of model compounds and of lysozyme by iodide ion, Biochemistry 10 (1971) 3254–3263.
[43] P.D. Ross, S. Subramanian, Thermodynamics of protein association reactions: forces contributing to stability, Biochemistry 20 (1981) 3096–3102.
[44] F. Zsila, Z. Bikadi, D. Malik, P. Hari, I. Pechan, A. Berces, E. Hazai, Evaluation of drug–human serum albumin binding interactions with support vector machine aided online automated docking, Bioinformatics 27 (2011) 1806–1813.
[45] L.M. Salonen, M. Ellermann, F. Diederich, Aromatic rings in chemical and biological recognition: energetics and structures, Angew. Chem. Int. Ed. 50 (2011) 4808–4842.
[46] C.C. Valley, A. Cembran, J.D. Perlmutter, A.K. Lewis, N.P. Labello, J. Gao, J.N. Sachs, The methionine-aromatic motif plays a unique role in stabilizing protein structure, J. Biol. Chem. 287 (42) (2012) 34979–34991.
[47] M. Senćanski, Lj. Došen-Mićović, V. Šukalović, S. Kostić-Rajačić, Theoretical insight into sulfur–aromatic interactions with extension to D2 receptor activation mechanism, Struct. Chem. 26 (2015) 1139–1149.